Hindawi Publishing Corporation
International Journal of Photoenergy
Volume 2013, Article ID 875456, 10 pages
http://dx.doi.org/10.1155/2013/875456

Research Article

Effect of Different Calcination Temperatures on the Structural and Photocatalytic Performance of Bi-TiO_2/SBA-15

Jing Ma,[1] Jia Chu,[2] Liangsheng Qiang,[3] and Juanqin Xue[1]

[1] *College of Metallurgical Engineering, Xi'an University of Architecture and Technology, Xi'an 710055, China*
[2] *College of Chemistry and Chemical Engineering, Xi'an University of Science and Technology, Xi'an 710054, China*
[3] *Department of Chemistry, Harbin Institute of Technology, Harbin 150001, China*

Correspondence should be addressed to Jing Ma; mjhit@yahoo.cn and Jia Chu; chujiahit@yahoo.cn

Received 17 May 2013; Revised 27 June 2013; Accepted 28 June 2013

Academic Editor: Huogen Yu

The new novel material Bi-TiO_2/SBA-15 was synthesized by an easy wet impregnation method. A combination of XRD, XPS, Raman, N_2 adsorption-desorption isotherm measurement, TEM, and solid state UV-Vis spectroscopy has been used to characterize the Bi-TiO_2/SBA-15 material. It was found that SBA-15 retained the ordered hexagonal mesostructure after incorporation of TiO_2 and Bi. The photodecomposition of rhodamine B (RhB) in aqueous medium was selected to evaluate the photocatalytic performance of Bi-TiO_2/SBA-15 under visible light irradiation ($\lambda \geq 420$ nm). The experiment results indicated that Bi-TiO_2/SBA-15 exhibited higher photocatalytic activities than pure TiO_2 and Bi_2O_3. The influences of calcination temperature were studied. It strongly influenced the activity of the samples. The sample calcined at 550°C shows the highest photocatalytic activity in the decomposition of RhB under visible light. The catalyst preserved almost its initial photocatalytic activity after six reuses.

1. Introduction

The photocatalytic properties of TiO_2 have been exploited in various applications since Fujishima and Honda reported a TiO_2 photochemical electrode for splitting water in 1972 [1]. TiO_2 is regarded as the most promising one for its high photocatalytic activity, chemical/photocorrosion stability, low cost, and environmental friendliness. However, the large band gap of TiO_2 (3.20 eV) and low quantum efficiency restricts its wide application [2]. This factor can be minimized by doping of semiconductors such as WO_3, Bi_2O_3, and CdS, which could change the electronic properties of TiO_2 [3–5]. Among them, Bi-based photocatalysts (Bi_2O_3 or its related compounds) have attracted much attention. Bi_2O_3 (2.8 eV) exhibits good charge carrier mobility, in which species with lone electron pair forming Bi-O polyhedra can act as electron trapping centers and hinder electron-hole pair recombination to improve the photoabsorptivity and photocatalytic activity [6, 7].

Recently, there are several works on the photocatalytic properties of Bi-doped TiO_2 materials under visible light irradiation [8–10]. Hou et al. used Bi_2O_3 quantum dots to enhance the photoactivity of TiO_2 nanosheets with exposed (001) facets [11]. Di Camillo et al. reported that Bi-doped TiO_2 NFs have been deposited by electrospinning and showed very interesting photocatalytic properties [12]. Su et al. synthesized a new TiO_2-based photocatalyst with both B doping and Bi_2O_3 coupling ($Bi_2O_3/TiO_{2-x}B_x$). The catalyst was used in degrading pentachlorophenol under visible light ($\lambda > 420$ nm) irradiation [13]. Li et al. reported the preparation of highly monodisperse spherical Bi-doped TiO_2. Their hybrid showed enhanced photocatalytic activity under visible light [14]. Shamaila et al. demonstrated an approach for the preparation of a mesoporous nanocrystalline TiO_2 based on EISA method [15]. The catalyst showed the superior activity as compared to M-TiO_2 (M refers to metal ion), Degussa P25, and impregnated Degussa P25 for the photodegradation of Methyl Orange (MO) and 2,4-dichlorophenol (2,4-DCP). Rengaraj and coworkers synthesized a Bi^{3+}-doped TiO_2 nanocatalyst. According to their results, the presence of Bi species in TiO_2 catalysts substantially enhanced the photocatalytic degradation of methyl parathion under UV irradiation [16].

Generally, the present Bi_2O_3-TiO_2 composite photocatalysts were limited by the low adsorption ability. To address this issue, much effort has been focused on enhancing the adsorption ability of the catalysts to improve their photocatalytic performance. Well-ordered mesoporous silica materials such as MCM-41 and SBA-15 have been widely used for adsorption, separation and catalysis [17–20]. SBA-15 is a type of uniform hexagonal pores and high surface area mesoporous material. Such type of highly interconnected mesostructured porous material is expected to allow the guest species to access the opened porous host easily. Design of photocatalysts modified by SBA-15 is a promising way to enhance high photocatalytic activity. However, no studies have attempted to establish a system consisting of a Bi_2O_3-TiO_2 hybrid incorporated into mesoporous silica.

Herein, the aim of the present paper is to investigate the synthesis of size controlled Bi_2O_3 and TiO_2 supported on mesostructured SBA-15. The photodegradation of RhB was employed to evaluate the photocatalytic activities of the Bi-TiO_2/SBA-15, with a 300 W Xe lamp ($\lambda \geq 420$ nm) as the light source.

Rhodamine B (RhB, N,N,N′,N′-tetraethylrhodamine) has moderate wash and light fastness properties. It is a useful analytical reagent for the detection and determination of metals. However, the use of RhB as a food color has been discontinued for a number of years on account of its suspected carcinogenic nature. Therefore, the removal of these dyes from wastewater is of great concern. Based on these considerations, the photodecomposition of RhB in aqueous medium was selected to evaluate the photocatalysis performance of Bi-TiO_2/SBA-15.

Considering the different calcination temperatures having an influence on the photocatalytic performance, the activities on different calcination temperatures were tested and discussed. Moreover, the recycle ability of Bi-TiO_2/SBA-15 was also evaluated.

2. Experimental

2.1. Catalyst Preparations. The SBA-15 was prepared according to the previous procedure by reaction from a solution of triblock copolymer P123 ($EO_{20}PO_{70}EO_{20}$, Aldrich) and tetraethoxysilane (TEOS) [21, 22]. P123 was used as a structure directing agent. In a typical process, 2 g of P123 was added to 75 mL of aqueous HCl under stirring at 40°C for 2 h. 4.17 mL of TEOS was then added to the solution which was stirred for another 24 h. The suspension was transferred into a steel autoclave and kept at 100°C for 72 h. After cooling to room temperature, the precipitate in the bottom of Teflon vessel was collected, filtered, thoroughly washed with water to remove any unreacted chemicals, and dried at room temperature. Calcinations were performed by heating in air at 550°C for 6 h to remove the template.

TiO_2/SBA-15 material was first prepared by internal hydrolysis method with little modification [23]. In this case, the calculated amount of tetrabutyl titanate (TBT) was dissolved in ethanol in a volume ratio of 1 : 5 (the amount of TBT is 0.92 mL). 0.5 g SBA-15 was then added to the solution containing TBT and stirred for 1 h to make the TBT adsorb completely on the SBA-15. The condensation reaction was started by dropwise addition of water and then the stirring was continued for 2 h to hydrolyze TBT completely. The solid product was recovered by filtration, washed with ethanol to remove any unanchored titanium species, dried at 80°C overnight, and calcined in air at 550°C for 3 h. The calcined samples were designated as TiO_2/SBA-15.

For Bi-doping TiO_2/SBA-15 supports, samples containing Bi were prepared by an easy wet impregnation method. TiO_2/SBA-15 and $Bi(NO_3)_3{\cdot}5H_2O$ were mixed in an ethanol solution with a drop of HNO_3 and stirred for 5 h, where the Bi/Ti molar ratio is 2.0%. The suspension was dried and calcined in air at different temperatures. The samples were designated as Bi-TiO_2/SBA-15(x), where x refers to the calcination temperatures, which are 400°C, 550°C, 700°C, and 850°C, respectively.

2.2. Characterization Techniques. Small-angle X-ray diffraction (SAXRD) measurements were performed on a Siemens D5005 instrument with CuKα ($\lambda = 0.154$ nm) radiation. The diffractograms were recorded in the 2ϑ range of 0.5–5° with a 2ϑ step size of 0.01°. Wide-angle X-ray diffraction (WAXRD) measurements were carried out on an XRD-6000 X-ray diffractometer (Shimadzu) CuKα ($\lambda = 0.154$ nm) radiation. The diffractograms were recorded in the 2ϑ range of 10–80° with a 2ϑ step size of 0.2°. Raman spectra were measured with JOBIN YVON HR800 Raman spectrophotometer (France) in the range of 100–1400 cm^{-1}, using an Ar ion laser. N_2 adsorption-desorption isotherms were measured at 77 K in a Quantachrome Autosorb-1 sorption analyzer. Samples were outgassed at 300°C for 10 h before the measurement. TEM was performed by an FEI Tecnai G2 S-Twin electron microscope with an acceleration voltage of 200 kV. XPS was obtained using a physical electronics model PHI5700 X-ray photoelectron spectrometer with MgKα X-rays as the excitation source. The binding energies were calibrated with reference to C1s at 285 eV. UV-V is absorption spectra scans were performed on a Shimadzu UV-2550 spectrometer in the range from 300 to 600 nm. $BaSO_4$ was used as a reflectance standard material during the experiment. Photoluminescence (PL) spectra were performed on JASCO FP-6500 fluorescence spectrometer.

2.3. Photocatalytic Activity Measurement. The photocatalytic activities were investigated for the photodegradation of RhB in aqueous solution under visible light in a photolysis glass reactor. The pH of solution was 7 during the reaction. The visible light source was a 300 W Xe lamp ($\lambda \geq 420$ nm to provide visible light irradiation) with a double wall jacket in which water was circulated to prevent overheating of the reaction mixture. 50 mg of Bi-TiO_2/SBA-15(x) was added to rhodamine B (RhB) (100 mL, 1×10^{-5} M) and stirred for 30 min without visible light irradiation in order to establish an adsorption-desorption equilibrium between RhB and the catalyst. Next, the solution was illuminated by visible light. At a given time interval, 4 mL of the suspension was withdrawn. After centrifugation at 5000 rpm for 5 min, the filtrate was monitored by UV-Vis spectrophotometer (UV-5200).

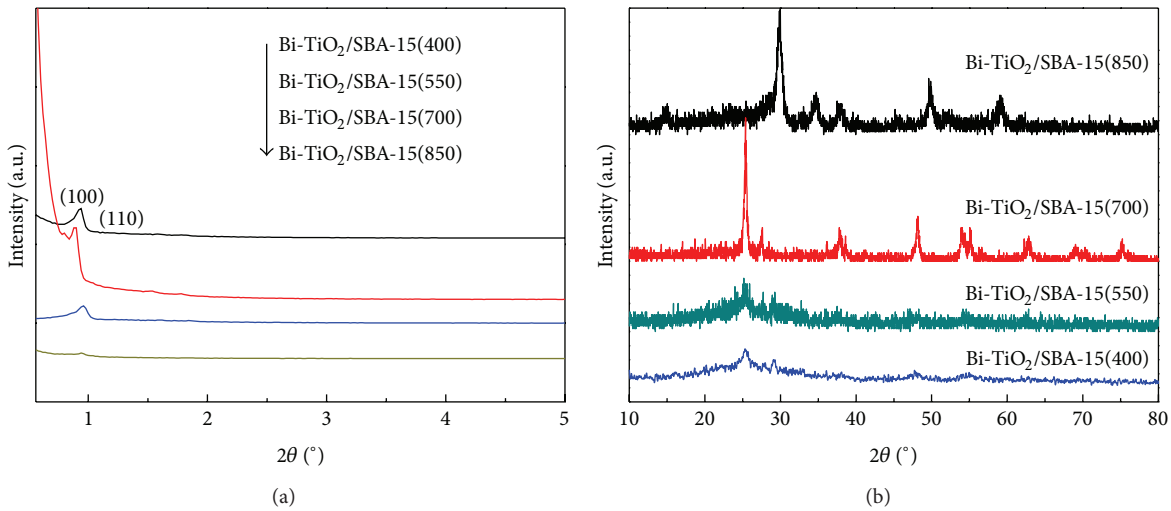

Figure 1: Small-angle (a) and wide-angle (b) XRD patterns of Bi-TiO_2/SBA-15(x).

Table 1: Textural properties of Bi-TiO_2/SBA-15(x).

Samples	Bi/Ti[a]	BET area ($m^2 \cdot g^{-1}$)	V_{tot}[b] ($cm^3 \cdot g^{-1}$)	D[c] (nm)
SBA-15	0	590.3	0.961	7.224
Bi-TiO_2/SBA-15(400)	2.01%	540.1	0.544	5.936
Bi-TiO_2/SBA-15(550)	1.95%	527.7	0.518	5.882
Bi-TiO_2/SBA-15(700)	1.89%	299.5	0.307	5.767
Bi-TiO_2/SBA-15(850)	1.62%	182.7	0.221	4.061
TiO_2/SBA-15(550)	0	568.3	0.924	6.818

[a]Bi/Ti was measured by ICP, [b]V_{tot}: the total pore volume, [c]D: average pore diameter.

3. Results and Discussions

3.1. Textural Properties and Characterization Typical. Small-angle XRD patterns of calcined Bi-TiO_2/SBA-15(x) samples in the range of 0.5–5° were shown in Figure 1(a). All samples exhibit well-resolved diffraction peak at $2\vartheta = 0.8$-$0.9°$ corresponding to the (100) diffraction peak of the hexagonal features of the SBA-15, indicating that their ordered pore structure is maintained well. The position of the diffraction peak shifted to a higher angle indicating a small decrease of the pore size and unit cell. It is seen that SBA-15 has a good thermal stability. The diffraction intensity gradually decreased with increasing the calcination temperature.

Figure 1(b) shows the wide-angle XRD pattern of the Bi-TiO_2/SBA-15(x) calcined at different calcination temperatures. The XRD patterns of the samples evidenced that when the temperature is 400 and 550°C, a typical broad diffraction peak centered at 2ϑ of 25°, which is typical characteristic of amorphous silica. No clear characteristic peaks of crystalline TiO_2 and Bi_2O_3 were observed in XRD patterns of sample, which indicated that the small nanoparticle sizes of TiO_2 and Bi_2O_3 were successfully incorporated into the silica framework. However, sample calcined at 700°C shows the appearance of anatase phase. It is observed that, with increase of calcination temperature, TiO_2 grain size increases. With further increase of calcination temperature to 850°C, a new diffraction peak at $2\vartheta = 30°$ was observed in the XRD pattern, which might be due to the formation a new phase of $Bi_4Ti_3O_{12}$ at 850°C. It is indicated that the new phase gradually dominates the composition of the samples. So it is feasible to control the ratio of the anatase phases by varying the calcination temperatures. In addition, no significant diffraction peak of Bi species was observed regardless of the calcination temperature because of the higher dispersion of Bi and the low content of Bi.

The adsorption-desorption isotherms for Bi-TiO_2/SBA-15 are shown in Figure 2(a). The samples exhibit isotherms of typical type IV with a H2 hysteresis loop due to the capillary condensation steps at relative pressure of $0.5 < p/p_0 < 0.8$, which is characteristic of a mesopores material [24, 25]. It can be clearly observed that the amount of N_2 adsorption decreases upon Bi_2O_3 and TiO_2 addition. Such a decrease of N_2 adsorption for samples is reasonable, considering the formation of Bi_2O_3 and TiO_2 nanoparticles inside the mesopores of SBA-15. When the calcination temperature increases to 850°C, the isotherm changes to H1 hysteresis loop. The hysteresis loop in the isotherms is obviously shifted to the high relative pressure, indicating that pore sizes of the samples decrease with the calcination temperature.

The BET specific area and the pore size of TiO_2/SBA-15 and Bi-TiO_2/SBA-15(x) were summarized in Table 1. The specific surface area, pore size, and volume decrease

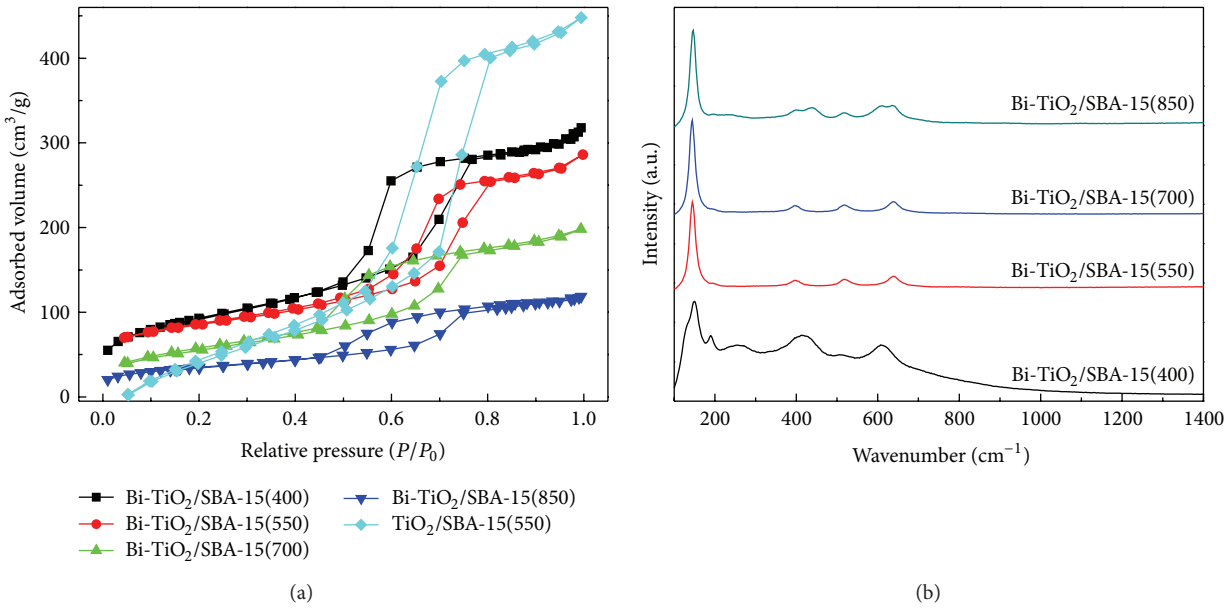

Figure 2: (a) N_2 adsorption-desorption isotherms of Bi-TiO_2/SBA-15(x). (b) Raman spectra of Bi-TiO_2/SBA-15(x).

with the calcination temperature increasing. Based on the observations, with the calcination temperature increasing, total pore volume and BET surface area were decreased 16.0% and 5.9% at least, respectively. It is clear that the increasing calcination temperature leads to decrease pore volume, specific surface area, and the porosity of the samples. Meanwhile, the increasing calcination temperature helps to increase the TiO_2 nanoparticles crystallization degree. We also noted that, when the temperature increased to 850°C, there was a mutation of the specific surface area, which was attributed to the new phase, obstructing the pores of the SBA-15.

Raman spectroscopy further verified the TiO_2 transformation for Bi-TiO_2/SBA-15(x), as shown in Figure 2(b). The Raman bands appear at 147, 400, 520, and 641 cm^{-1} and can be assigned to the E_g, B_{1g}, A_{1g}, and B_{1g} vibration modes of anatase TiO_2 [26]. The results indicate that the doping of Bi has not influenced the anatase type of TiO_2. A new peak appears at 200 cm^{-1} when the calcination temperature was 400°C, which is attributed to the brookite phase. When the temperature is higher, the TiO_2 in brookite phase has been full conversion to anatase with improving the crystalline. When the calcination temperature is up to 850°C, TiO_2 is still in anatase phase in the samples with partial conversion to a new phase of $Bi_4Ti_3O_{12}$. It is indicated that the introduction of Bi can inhibit the transformation of TiO_2 phase in the high temperature.

Figure 3 shows that it retains a regular hexagonal array of uniform channels characteristic of SBA-15 with Bi and TiO_2. It displays highly ordered hexagonal regularity mesopores, where nanoparticles are embedded in the pore walls with random orientation. When the calcination temperature is up to 850°C, the nanocrystals structures do not change and slightly increased the nanoparticles size derived from XRD data. After the same treatment (up to 850°C), the crystal domain size of TiO_2 increased with partial conversion to $Bi_4Ti_3O_{12}$ and that of Bi_2O_3 crystals increased with partial conversion to monoclinic modification.

HRTEM image (Figure 3(e)) reveals that the materials were well crystallized, as evidenced by well-defined lattice fringes. The lattice fringes of 0.35 nm match the (101) plane of anatase TiO_2, while that of 0.325 nm match the (120) plane of Bi_2O_3 nanoparticles, respectively. The HRTEM analysis confirmed that Bi_2O_3 and TiO_2 coexisted in the resulting samples.

In order to analyze the chemical composition and purity of the prepared particles, the XPS survey spectrum of Bi-TiO_2/SBA-15 is shown in Figure 4. Figure 4(a) shows that Bi-TiO_2/SBA-15 contains only Ti, O, Bi, Si, and C elements. The C element can be ascribed to the residual carbon from our characterization. The high-resolution XPS spectra of Bi4f are shown in Figure 4(b). The peaks of Bi 4f7/2 and Bi 4f5/2 are centered at 159.3 and 164.5 eV, which is in agreement with Bi_2O_3 values of other observations [27, 28]. After calcinations at higher temperature, these two peaks move a little to lower energies, hinting that bismuth element brings more effective positive charge and tends to convert to its stable oxidation state from +3 to 0. The Bi species would segregate from the shallow surface and move onto the photocatalyst surface, and some Bi^0 species are oxidized into Bi^{3+} species. This means that calcination may lead to more Bi_2O_3 species formed and to segregation on photocatalyst surface. A weak signal centred at 157.2 eV indicated the existence of Bi^0 [29].

The XPS spectra of O 1s are shown in Figure 4(c). The O 1s peak is broad and complicated due to the nonequivalence of oxygen ions. The peak shape suggests that it is composed of multiple peaks that arise due to the overlapping contributions of oxide ions. The strong peak at 529.8 eV is ascribed to Ti–O bond in TiO_2, the peak at 531.4 eV, which is assigned to the oxygen attached to bismuth (Bi–O bond), and

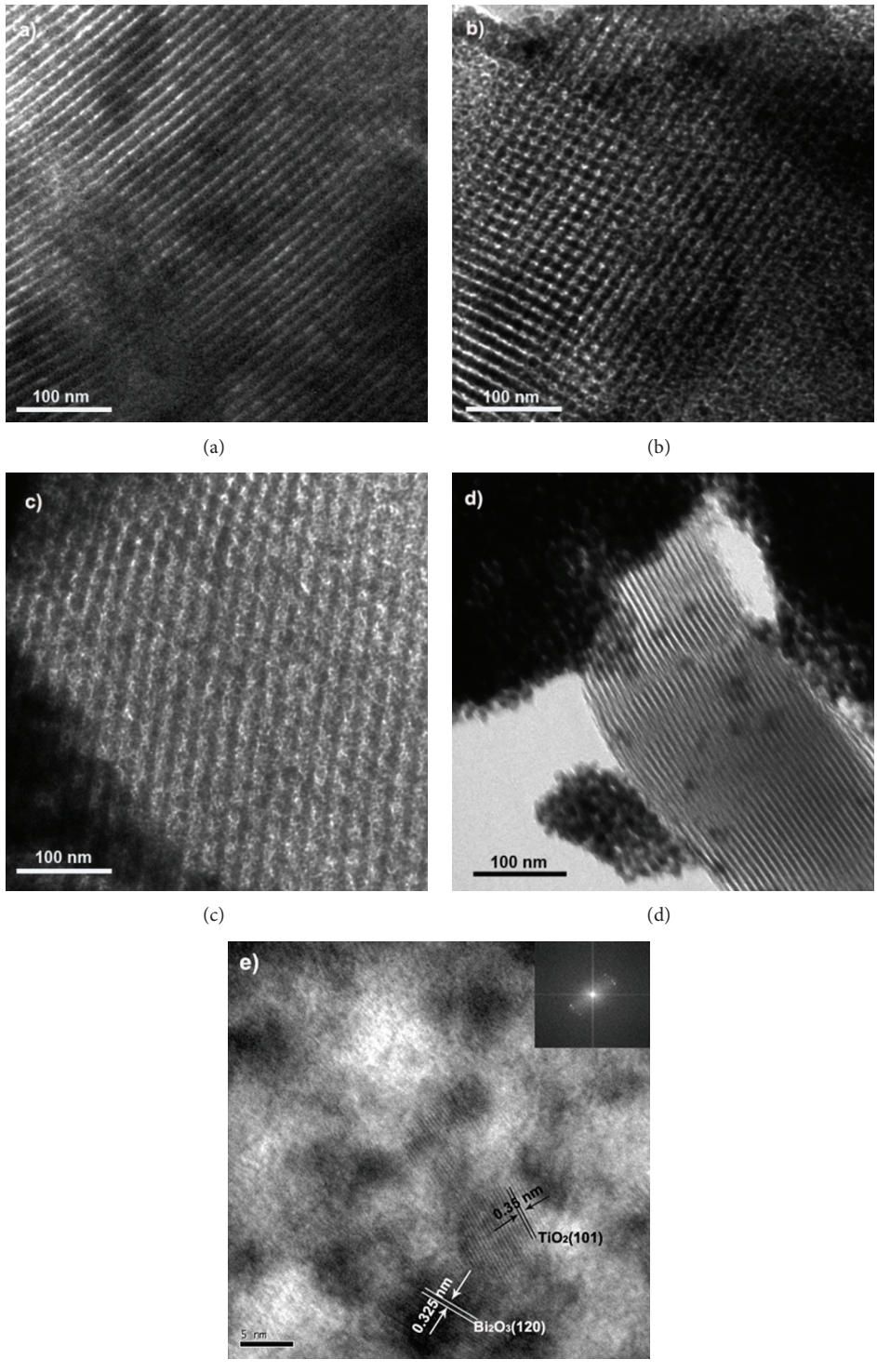

Figure 3: TEM images of Bi-TiO_2/SBA-15: (a) Bi-TiO_2/SBA-15(400), (b) Bi-TiO_2/SBA-15(550), (c) Bi-TiO_2/SBA-15(700), (d) Bi-TiO_2/SBA-15(850), and (e) HRTEM image of Bi-TiO_2/SBA-15(550) (inset is the corresponding FFT pattern).

the shoulder at 533.6 eV is attributed to the OH^- group absorbed on the surface. The Ti 2p of Bi-TiO_2/SBA-15 is shown in Figure 4(d). The peaks of Ti2p3/2 and Ti2p1/2 were centered at 458.2 and 464.7 eV, which showed that the main valence of Ti in the prepared catalysts is +4 and Ti^{4+} is in tetrahedral coordination with oxygen in the catalysts. Meanwhile, there was no significant influence on the spectra in either Ti 2p or O 1s in the presence of Bi_2O_3.

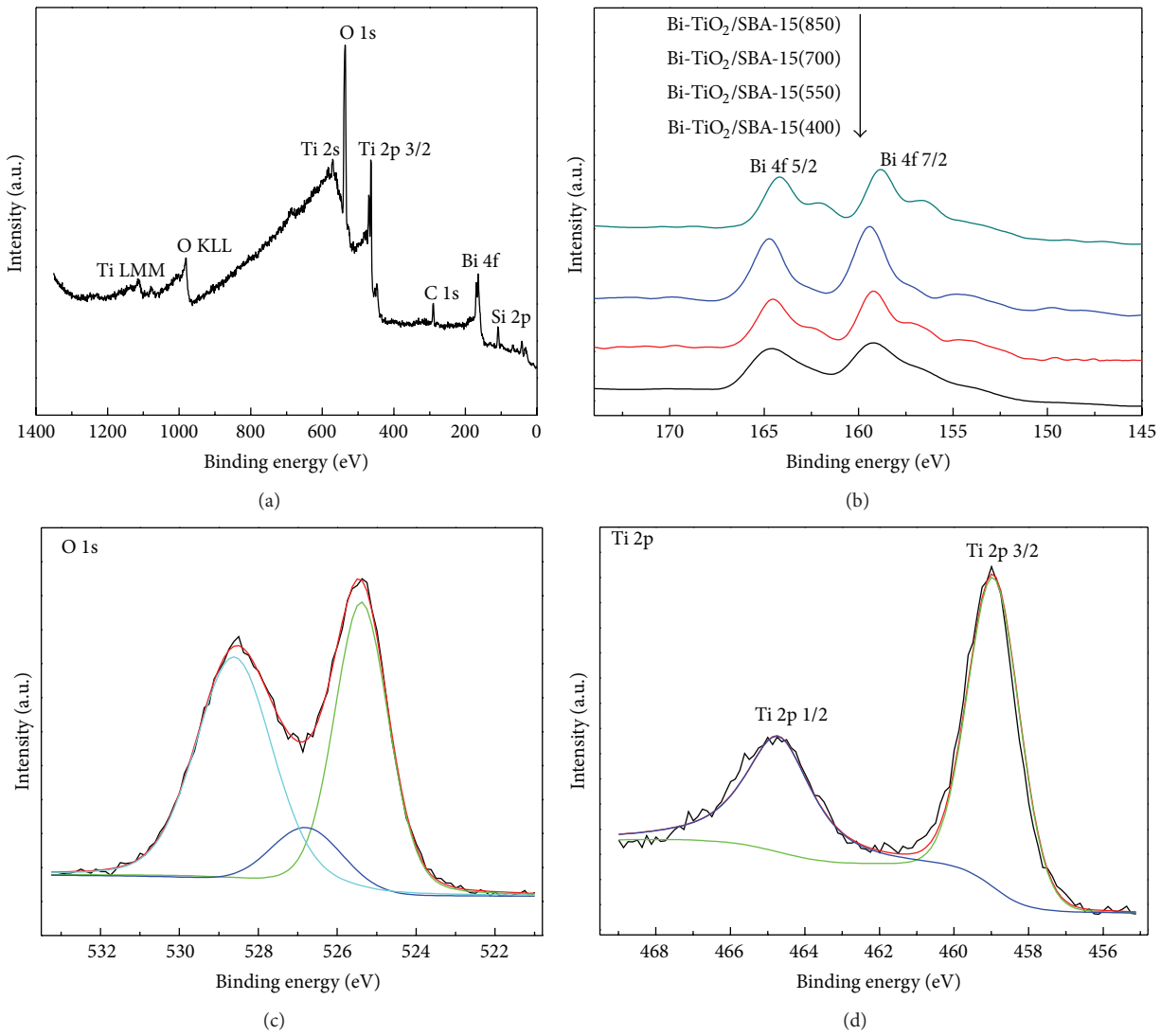

FIGURE 4: XPS survey spectrum of Bi-TiO_2/SBA-15 (a), the high-resolution XPS spectra of Bi 4f region (b), O 1s (c), and Ti 2p (d).

The UV-Vis absorption spectra of the Bi-TiO_2/SBA-15 were presented in Figure 5(a). There a red shift for Bi-TiO_2/SBA-15 in the visible region. The results show that the doping of Bi can increase the absorbance of visible light and extend the absorption edge to longer wavelengths. It can be seen that the Bi-TiO_2/SBA-15 calcined at 400–700°C displayed similar absorbance for visible lights, suggesting that, in the composite, Bi_2O_3 mainly resulted in the spectral response in the visible region. However, with the increase of calcination temperature to 850°C, the Bi-TiO_2/SBA-15 showed an obviously stronger absorption in the visible light region than that of calcined at other temperatures, which might be due to the formation of a new phase of $Bi_4Ti_3O_{12}$ at 850°C. Moreover, the plot of $(\alpha h\nu)^{1/2}$ versus the energy of light afforded band gap energy of 2.81 eV for Bi-TiO_2/SBA-15 (see the inset in Figure 5(a)), which could be easily induced photoelectrons and holes by visible lights.

PL emission spectra have been used to investigate the efficiency of charge carrier trapping, immigration, transfer and to understand the fate of electron-hole pairs in semiconductor particles [30]. Figure 5(b) showed the PL spectra of TiO_2 and Bi-TiO_2/SBA-15 in the range of 400–525 nm. The PL intensity of the samples decreases as follows: TiO_2 > Bi-TiO_2/SBA-15(400) > Bi-TiO_2/SBA-15(700) > Bi-TiO_2/SBA-15(850) > Bi-TiO_2/SBA-15(550). It indicated that, when increasing the calcination temperature, the decrease in trap states on samples surface may slow the recombination process of photogenerated electrons and holes in TiO_2, which benefit the photocatalytic reaction.

3.2. The Photocatalytic Activity of Bi-TiO_2/SBA-15. The UV-Vis absorption spectra clearly reveal that the visible light absorption of Bi-TiO_2/SBA-15 is higher than that of TiO_2. Therefore, it is reasonable to expect higher photocatalytic activity when the Bi species and TiO_2 deposited on the SBA-15 mesostructure. We evaluated the Bi-TiO_2/SBA-15(x) samples for degradation of RhB under visible light irradiation and compared the catalytic efficiency of Bi-TiO_2/SBA-15(x) with

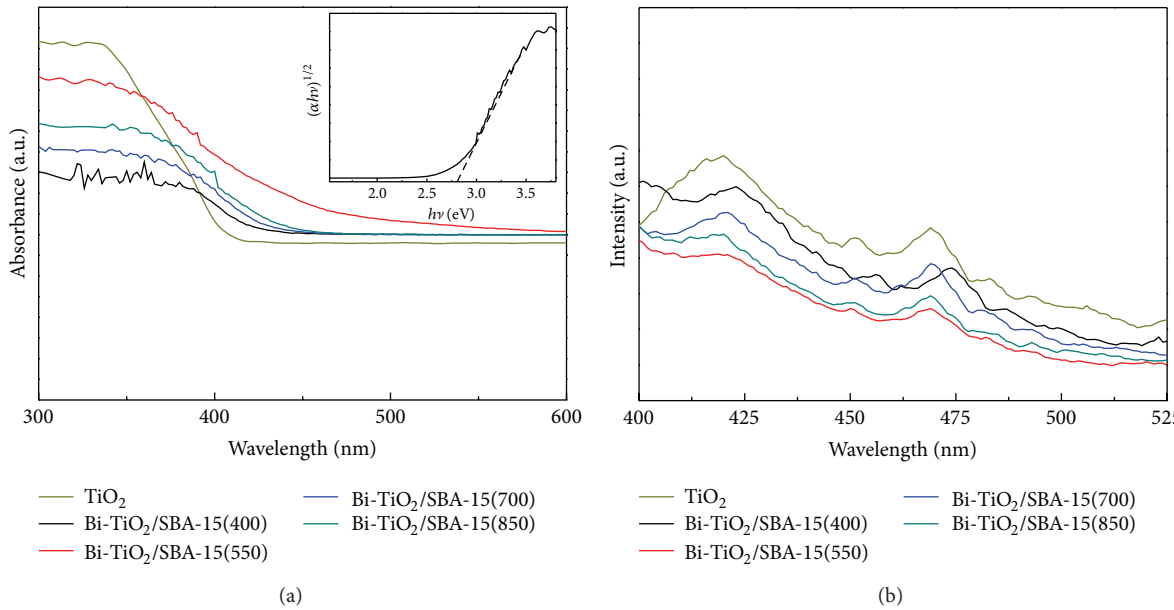

FIGURE 5: UV-Vis absorption spectra (a) and PL spectra of Bi-TiO_2/SBA-15 (b).

that of TiO_2. The photoactivities for RhB in dark in the presence of the photocatalyst under visible light irradiation in the absence of the photocatalyst are evaluated. It is found that there was no degradation for the RhB in the dark and in the presence of the photocatalyst. There is no degradation observed for RhB when the solution is placed under visible light radiation without the addition of photocatalysts.

Figure 6(a) displayed the effect of the calcination temperature on the photocatalytic activity. The activities decrease showed in the following order: Bi-TiO_2/SBA-15 (550) > Bi-TiO_2/SBA-15(850) > Bi-TiO_2/SBA-15(700) > Bi-TiO_2/SBA-15(400) > Bi_2O_3/SBA-15 > TiO_2/SBA-15(550) > Bi_2O_3 >TiO_2.

It is well known that pure TiO_2 and TiO_2/SBA-15 have no photocatalytic activity under visible light irradiation. However, in Figure 6(a), the experiment results show a little decomposition ability of RhB, which is due to the small size of TiO_2 nanoparticles improving the photocatalytic activity. The degradation efficiency by Bi_2O_3/SBA-15 and Bi_2O_3 is also low.

The Bi-TiO_2/SBA-15(x) almost decomposed the RhB solution within 90 min, compared to the TiO_2 sample, which implies that the doped Bi is essential as a cocatalyst for the efficient degradation. That is to say, the Bi doping on TiO_2/SBA-15 is accorded to the higher photodegradation, which resulted from the formation of Bi species enhancing the electron and hole separation by capturing the photoinduced charges efficiently. There are two reasons for the superior photocatalytic performance. Firstly, valence band (VB) composed of hybridized Bi 6s, Ti 3d, and O 2p orbitals has a strong oxidizing ability and can effectively degrade organic pollutants. And the hybridization of the Bi 6s, Ti 3d, and O 2p levels makes the VB largely dispersed, which favors the mobility of photoholes in the VB and is beneficial for the oxidation reaction. Secondly, the assembled Bi_2O_3 increases the mobility of the photogenerated carriers, and good crystallization may lead to the enhancement of photocatalytic activity for the decomposition of the organic compounds. It is allowing more opportunities for electrons to participate in the reduction reaction to form active oxygen species. The transfer of the photoexcited electrons from the surface of Bi_2O_3 to TiO_2 occurs due to the small Bi_2O_3 band gap and its higher conduction band potential compared to that of TiO_2.

It is known that photodegradation kinetics follow Langmuir-Hinshelwood kinetics model [31]. The reaction can be represented as follows (1):

$$\ln \frac{C_0}{C} = k_{app} t, \tag{1}$$

where k_{app} is the apparent first-order reaction constant and C_0 is the initial concentration of the RhB solution. A kinetic linear simulation curve of RhB photocatalytic degradation using Bi-TiO_2/SBA-15(x) is shown in Figure 6(b). The fact that the curve showed good linearity indicating that the photocatalytic degradation of RhB using Bi-TiO_2/SBA-15(x) as catalyst fits well with the first-order reaction kinetics. The rate constant of Bi-TiO_2/SBA-15(x) for RhB photodegradation is shown in Table 2. k_{app} value of the Bi-TiO_2/SBA-15(550) is 0.0212 min^{-1}, which is higher than that of TiO_2 and other samples of Bi-TiO_2/SBA-15. It suggested that k_{app} improved by Bi doping. It is widely accepted that the high calcination temperature usually results in smaller specific surface area and particle size, as illustrated in Table 1. The calcination temperature strongly influenced the activity of the samples. Though the sample calcined at 400°C has the largest BET surface area and particle size, its crystalline is worse than that of the calcined at higher temperature, leading to lower photoactivity. Meanwhile, the effect of the photocatalytic activity is decreased when the calcination temperature is up to 700–850°C. It can be explained that the high calcination

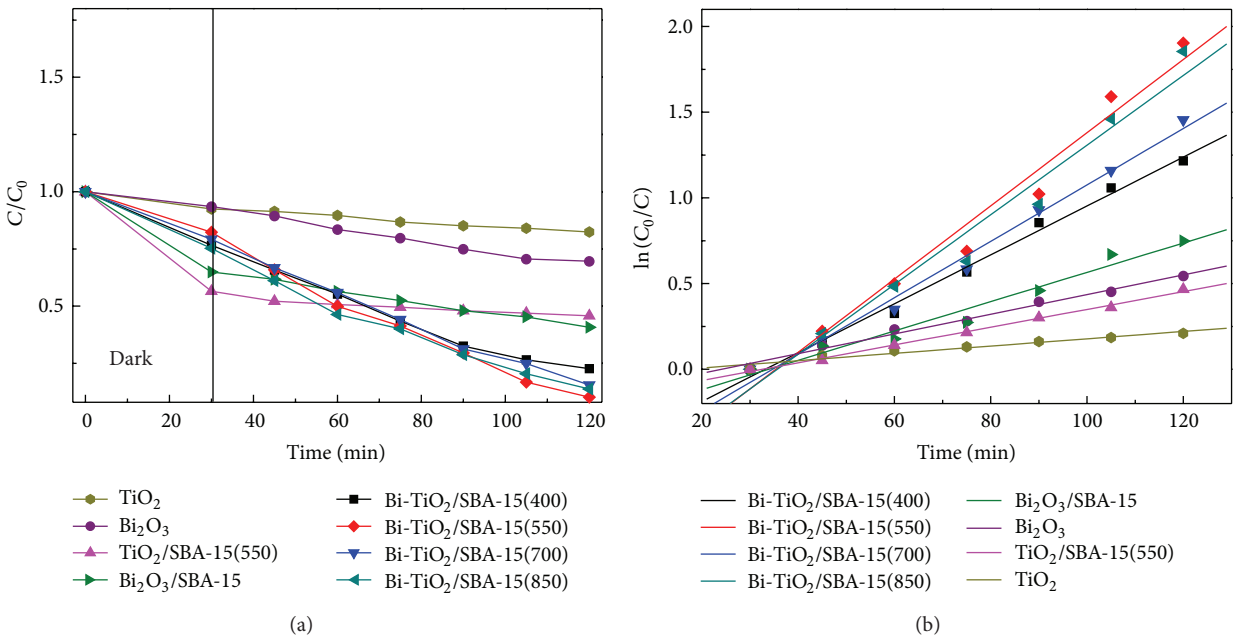

Figure 6: Photocatalytic activity (a) and kinetic linear simulation curve (b) of photocatalytic degradation by Bi-TiO_2/SBA-15(x) under visible light.

Table 2: The rate constant of Bi-TiO_2/SBA-15(x) for RhB photodegradation.

Samples	k_{app} (min^{-1})
Bi-TiO_2/SBA-15(400)	0.0135
Bi-TiO_2/SBA-15(550)	0.0212
Bi-TiO_2/SBA-15(700)	0.0162
Bi-TiO_2/SBA-15(850)	0.0206
Bi_2O_3/SBA-15	0.00818
TiO_2/SBA-15(550)	0.00553
Bi_2O_3	0.00755
TiO_2	0.00540

temperature destructed pore structure and caused loss in surface area to some extent, reducing the oxygen vacancies. The samples at 850°C show better photocatalytic activity than samples at 700°C, which might be due to the formation of a new phase of $Bi_4Ti_3O_{12}$ having higher photocatalytic activity. The sample calcined at 550°C shows the highest photocatalytic activity in the decomposition of RhB under visible light. Furthermore, the doping of Bi could effectively limit the phase transformation, preventing the overgrowth of crystallites and enhancing the visible light absorption in comparison with TiO_2 and TiO_2/SBA-15.

In addition, the Bi-TiO_2/SBA-15 obtained at 550°C presents the highest photocatalytic activity. However, as an excellent catalyst, it should not only show higher activity but also present stability in recycle process. As shown in Figure 7, Bi-TiO_2/SBA-15 can preserve most of its catalytic activity after six cycles and this confirms that the as-prepared Bi-TiO_2/SBA-15 is stable under irradiation for photocatalytic decomposition of organic pollutants.

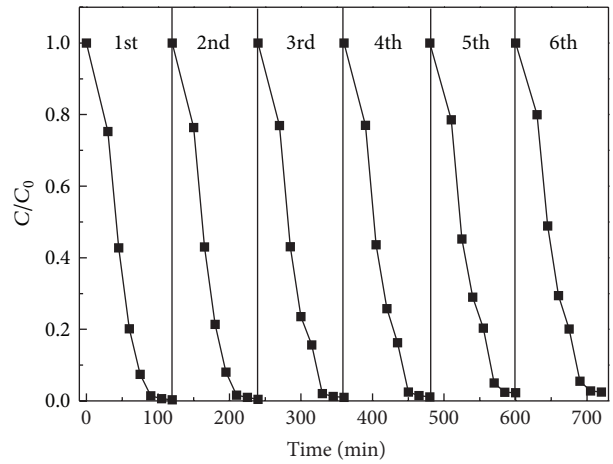

Figure 7: Recycling photocatalytic test of Bi-TiO_2/SBA-15 calcined at 550°C.

4. Conclusions

In conclusion, we have fabricated a visible photocatalyst Bi-TiO_2/SBA-15 material. The photocatalytic activity of the prepared photocatalysts was investigated by the photodegradation of RhB. A combination of XRD, XPS, Raman, nitrogen adsorption-desorption isotherm measurement, TEM, and UV-Vis absorption spectra has been used to characterize the Bi-TiO_2/SBA-15 material. The experiment results indicated that the Bi doping could enhance the photocatalytic activities than TiO_2. The calcination temperature strongly influenced the activity of the samples. The sample calcined at 550°C shows the highest photocatalytic activity in the decomposition of RhB under visible light. This work provides a new

pathway to design and fabricate novel photoactive materials for practical application in environmental cleaning.

Conflict of Interests

The authors declare that they do not have any commercial or associative interests that represents a conflict of interest directly or indirectly in connection with our work.

Acknowledgments

The authors are grateful for the financial support from the National Natural Science Foundation of China (no. 50978212), the State Key Program of Shaanxi Province Natural Science Foundation Project (no. 2012JZ7003), the Shaanxi Province Science and Technology and Innovation Project Foundation (no. 2011KTDZ01-05-05), and the Science Foundation from Education Department of Shaanxi Provincial Government (no. 2013JK0885 and no. 2013JK0650).

References

[1] A. Fujishima and K. Honda, "Electrochemical photolysis of water at a semiconductor electrode," *Nature*, vol. 238, no. 5358, pp. 37–38, 1972.

[2] J. Zhang, Z. Xiong, and X. S. Zhao, "Graphene-metal-oxide composites for the degradation of dyes under visible light irradiation," *Journal of Materials Chemistry*, vol. 21, no. 11, pp. 3634–3640, 2011.

[3] Y. Wang, R. Shi, J. Lin, and Y. Zhu, "Enhancement of photocurrent and photocatalytic activity of ZnO hybridized with graphite-like C_3N_4," *Energy and Environmental Science*, vol. 4, no. 8, pp. 2922–2929, 2011.

[4] Q. Y. Li, T. Kako, and J. H. Ye, "WO_3 modified titanate network film: highly efficient photo-mineralization of 2-propanol under visible light irradiation," *Chemical Communications*, vol. 46, no. 29, pp. 5352–5354, 2010.

[5] R. Li, W. Chen, H. Kobayashi, and C. Ma, "Platinum-nanoparticle-loaded bismuth oxide: an efficient plasmonic photocatalyst active under visible light," *Green Chemistry*, vol. 12, no. 2, pp. 212–215, 2010.

[6] J. Wang, Q. Cai, H. Li, Y. Cui, and H. Wang, "A review on TiO_2 nanotube film photocatalysts prepared by liquid-phase deposition," *International Journal of Photoenergy*, vol. 2012, Article ID 702940, 11 pages, 2012.

[7] H. Chen, J. Li, Q. Chen, D. Li, and B. Zhou, "Photoelectrocatalytic performance of benzoic acid on TiO_2 nanotube array electrodes," *International Journal of Photoenergy*, vol. 2013, Article ID 567426, 7 pages, 2013.

[8] Y. Wang, Y. Wang, Y. Meng et al., "A highly efficient visible-light-activated photocatalyst based on bismuth- and sulfur-codoped TiO_2," *Journal of Physical Chemistry C*, vol. 112, no. 17, pp. 6620–6626, 2008.

[9] L. Q. Jing, J. Wang, Y. C. Qu, and Y. B. Luan, "Effects of surface-modification with Bi_2O_3 on the thermal stability and photoinduced charge property of nanocrystalline anatase TiO_2 and its enhanced photocatalytic activity," *Applied Surface Science*, vol. 256, no. 3, pp. 657–663, 2009.

[10] Y. Q. Wu, G. X. Lu, and S. B. Li, "The doping effect of Bi on TiO_2 for photocatalytic hydrogen generation and photodecolorization of rhodamine B," *Journal of Physical Chemistry C*, vol. 113, no. 22, pp. 9950–9955, 2009.

[11] J. Hou, C. Yang, Z. Wang, S. Jiao, and H. Zhu, "Bi_2O_3 quantum dots decorated anatase TiO_2 nanocrystals with exposed (001) facets on graphene sheets for enhanced visible-light photocatalytic performance," *Applied Catalysis B*, vol. 129, pp. 333–341, 2013.

[12] D. Di Camillo, F. Ruggieri, S. Santucci, and L. Lozzi, "N-doped TiO_2 nanofibers deposited by electrospinning," *Journal of Physical Chemistry C*, vol. 116, pp. 18427–18431, 2012.

[13] K. Su, Z. Ai, and L. Zhang, "Efficient visible light-driven photocatalytic degradation of pentachlorophenol with Bi_2O_3/TiO_2-xBx," *Journal of Physical Chemistry C*, vol. 116, pp. 17118–17123, 2012.

[14] H. Y. Li, D. J. Wang, P. Wang, H. Fan, and T. Xie, "Synthesis and studies of the visible-light photocatalytic properties of near-monodisperse Bi-doped TiO_2 nanospheres," *Chemistry*, vol. 15, no. 45, pp. 12521–12527, 2009.

[15] S. Shamaila, A. K. L. Sajjad, F. Chen, and J. L. Zhang, "Study on highly visible light active Bi_2O_3 loaded ordered mesoporous titania," *Applied Catalysis B*, vol. 94, no. 3-4, pp. 272–280, 2010.

[16] S. Rengaraj, X. Z. Li, P. A. Tanner, Z. F. Pan, and G. K. H. Pang, "Photocatalytic degradation of methylparathion—an endocrine disruptor by Bi^{3+}-doped TiO_2," *Journal of Molecular Catalysis A*, vol. 247, no. 1-2, pp. 36–43, 2006.

[17] W. J. J. Stevens, K. Lebeau, M. Mertens, G. Van Tendeloo, P. Cool, and E. F. Vansant, "Investigation of the morphology of the mesoporous SBA-16 and SBA-15 materials," *Journal of Physical Chemistry B*, vol. 110, no. 18, pp. 9183–9187, 2006.

[18] C.-C. Yang, J. Vernimmen, V. Meynen, P. Cool, and G. Mul, "Mechanistic study of hydrocarbon formation in photocatalytic CO_2 reduction over Ti-SBA-15," *Journal of Catalysis*, vol. 284, no. 1, pp. 1–8, 2011.

[19] S. C. Zhang, D. Jiang, T. Tang et al., "TiO_2/SBA-15 photocatalysts synthesized through the surface acidolysis of $Ti(OnBu)_4$ on carboxyl-modified SBA-15," *Catalysis Today*, vol. 158, no. 3-4, pp. 329–335, 2010.

[20] V. Tajer-Kajinebaf, H. Sarpoolaky, and T. Mohammadi, "Synthesis of nanostructured anatase mesoporous membranes with photocatalytic and separation capabilities for water ultrafiltration process," *International Journal of Photoenergy*, vol. 2013, Article ID 509023, 11 pages, 2013.

[21] D. Zhao, J. Feng, Q. Huo et al., "Triblock copolymer syntheses of mesoporous silica with periodic 50 to 300 angstrom pores," *Science*, vol. 279, no. 5350, pp. 548–552, 1998.

[22] D. Zhao, Q. Huo, J. Feng, G. H. Fredrickson, and G. D. Stucky, "Nonionic triblock and star diblock copolymer and oligomeric sufactant syntheses of highly ordered, hydrothermally stable, mesoporous silica structures," *Journal of the American Chemical Society*, vol. 120, no. 24, pp. 6024–6036, 1998.

[23] J. Ma, J. Chu, L. S. Qiang, and J. Xue, "Synthesis and structural characterization of novel visible photocatalyst Bi-TiO_2/SBA-15 and its photocatalytic performance," *RSC Advances*, vol. 2, pp. 3753–3758, 2012.

[24] S. Y. Chai, Y. J. Kim, M. H. Jung, A. K. Chakraborty, D. Jung, and W. I. Lee, "Heterojunctioned BiOCl/Bi_2O_3, a new visible light photocatalyst," *Journal of Catalysis*, vol. 262, no. 1, pp. 144–149, 2009.

[25] Q. S. Huo, R. Leon, P. M. Petroff, and G. D. Stucky, "Mesostructure design with gemini surfactants: supercage formation in

a three-dimensional hexagonal array," *Science*, vol. 268, no. 5215, pp. 1324–1327, 1995.

[26] Y. J. Acosta-Silva, R. Nava, V. Hernández-Morales, S. A. Macías-Sánchez, M. L. Gómez-Herrera, and B. Pawelec, "Methylene blue photodegradation over titania-decorated SBA-15," *Applied Catalysis B*, vol. 110, pp. 108–117, 2011.

[27] S. Perathoner, P. Lanzafame, R. Passalacqua, G. Centi, R. Schlögl, and D. S. Su, "Use of mesoporous SBA-15 for nanostructuring titania for photocatalytic applications," *Microporous and Mesoporous Materials*, vol. 90, no. 1–3, pp. 347–361, 2006.

[28] J. J. Xu, Y. H. Ao, D. G. Fu, and C. Yuan, "Synthesis of Bi_2O_3-TiO_2 composite film with high-photocatalytic activity under sunlight irradiation," *Applied Surface Science*, vol. 255, no. 5, pp. 2365–2369, 2008.

[29] M.-W. Chu, M. Ganne, M. T. Caldes, and L. Brohan, "X-ray photoelectron spectroscopy and high resolution electron microscopy studies of Aurivillius compounds: $Bi_{4-x}La_XTi_3O_{12}$($x = 0$, 0.5, 0.75, 1.0, 1.5, and 2.0)," *Journal of Applied Physics*, vol. 91, no. 5, pp. 3178–3187, 2002.

[30] Y. Z. Li and S.-J. Kim, "Synthesis and characterization of nano titania particles embedded in mesoporous silica with both high photocatalytic activity and adsorption capability," *Journal of Physical Chemistry B*, vol. 109, no. 25, pp. 12309–12315, 2005.

[31] S. Zheng, Y. Cai, and K. E. O'Shea, "TiO_2 photocatalytic degradation of phenylarsonic acid," *Journal of Photochemistry and Photobiology A*, vol. 210, no. 1, pp. 61–68, 2010.